

Modeling of plasma turbulence and transport in LAPD

P. Popovich, M.V. Umansky*, T. A. Carter, and B. Friedman

Department of Physics and Astronomy, University of California,
Los Angeles, California 90095-1547, USA

*Lawrence Livermore National Laboratory,
Livermore, CA 94550, USA

July 12, 2022

Abstract

A numerical model of plasma turbulence is applied to the Large Plasma Device (LAPD) (Gekelman et al, Rev. Sci. Inst., 62, 2875, 1991). The model, implemented in the BOUT code, includes 3-D collisional fluid equations for plasma density, electron parallel momentum, and current continuity, and it includes the effects of ion-neutral collisions. In nonlinear simulations, self-consistent evolution of turbulence and turbulence-generated zonal flows results in saturated turbulence which in many ways is very similar to the experiment. Among these, the frequency spectra, spatial correlation, and probability distribution of fluctuation amplitude from the code appear in remarkably good agreement with LAPD measurements.

To be submitted for publication

1 Introduction

Plasma turbulence is a truly ubiquitous phenomenon, given that most of universe is in the plasma state, and most plasmas are turbulent. Over last several decades, plasma turbulence has been the subject of intense research in space and astrophysical plasmas, and in laboratory plasmas in a number of areas: fusion, plasma processing, thrusters, and beyond. Similar to neutral hydrodynamics, plasma turbulence remains an "unsolved" problem in the sense that clear physical understanding of the observed phenomena does not exist. A few reduced models of plasma turbulence, such as the Hasegawa-Mima [1, 2] and Hasegawa-Wakatani [3], have been successful in clarifying certain aspects of plasma turbulence. However, for practically interesting situations a numerical simulation is often the only solution method.

Linear machines are relatively simple experimental devices used for exploring basic plasma physics: turbulence, transport, waves, atomic physics, plasma-material interactions [4, 5, 6, 7].

Linear plasma devices are of particular interest to fusion edge plasma community since plasma parameters in linear devices are often similar to those in the boundary region of tokamaks.

A relatively new aspect of linear devices is using them for validating many aspects of plasma modeling codes. This in part motivated several recent studies where plasma turbulence codes were applied to linear devices [8, 9, 10, 11].

The Large Plasma Device (LAPD) is a versatile linear plasma machine used for range of experimental studies: plasma turbulence, transport, waves, reconnection and others [4]. Due to its large length LAPD is similar to tokamak SOL in the sense that the radial plasma density and temperature profiles are determined by the competition of the radial turbulent transport, parallel streaming, and volumetric sources.

LAPD is a particularly interesting object for numerical modeling due detailed turbulence diagnostics and extensive experimental studies of plasma turbulence [12, 13]. Applications of numerical models to plasma turbulence in LAPD have been attempted previously []. In a new computational study described further in this report, a rather detailed comparison is conducted for numerically calculated plasma turbulence and a broad range of experimental turbulence characteristics in LAPD.

2 Physics model

The LAPD device at UCLA is a long cylindrical plasma configuration with length $L = 18$ m, vacuum vessel radius $r_s=50$ cm, typical plasma radius $a \sim 40$ cm, electron density $n_{e0} \sim 2..5 \times 10^{12}$ cm $^{-3}$, electron temperature $T_e \lesssim 10$ eV, and ion temperature $T_i \lesssim 1$ eV; with an externally imposed axial magnetic field magnetic field $B_z < 0.25$ T. It usually runs He plasmas, singly ionized for this temperature.

For the calculations discussed further, this configuration is modeled as a cylindrical annulus, with inner radius 15 cm and outer radius 45 cm. The magnetic field is taken uniform, along the cylinder axis, and the axial boundary conditions are taken periodic. For more details on the geometry and numerical implementation of BOUT in application to LAPD see [14].

For drift-type modes, LAPD plasmas are strongly collisional ($\nu_{ei}/\omega_* \gg 1$ and $\lambda_{ei}/L_{\parallel} \ll 1$), providing justification for a fluid model.

For the simulations described here we are using the following set of equations:

$$\partial_t N = -\mathbf{v}_E \cdot \nabla N - v_{\parallel e} N \quad (1)$$

$$\partial_t v_{\parallel e} = -\mathbf{v}_E \cdot \nabla v_{\parallel e} - \mu \frac{T_e}{N} \nabla_{\parallel} N + \mu \nabla_{\parallel} \phi - \nu_e v_{\parallel e} \quad (2)$$

$$\partial_t \varpi = -\mathbf{v}_E \cdot \nabla \varpi - \nabla_{\parallel} (N v_{\parallel}) + \mathbf{b} \times \nabla N \cdot \nabla \mathbf{v}_E^2 / 2 - \nu_{in} \varpi + \mu_i \nabla_{\perp}^2 \varpi \quad (3)$$

Here N is the plasma density, $v_{\parallel e}$ is the electron fluid parallel velocity, and ϖ is the potential vorticity introduced as

$$\varpi \stackrel{\text{def}}{=} \nabla_{\perp} \cdot (N \nabla_{\perp} \phi) \quad (4)$$

While the variables N , $v_{\parallel e}$ and ϖ are advanced in time, equation (4) is solved to reconstruct the perturbed potential ϕ from ϖ . In the code version used in this work, Eq. (4) is linearized to increase the calculation speed, since this equation has to be solved for each evaluation of the right-hand side of Eqs. (1-3). The vorticity evolution equation (3) replaces the current continuity equation. Derivation and discussion of this form of equation is presented in our paper discussing linear verification [14]. Derivation of the viscosity term is discussed in Appendix A.

The equations are implemented in the numerical code BOUT originally developed in the late 1990s for modeling of tokamak edge [15], the currently used version is described in detail in [16].

3 Turbulent transport and average density profile

3.1 Average and local fluctuating fields

Consider a fluctuating field $f(\vec{r}, t)$. For statistically steady turbulence it is convenient to represent f at any spatial location as a sum of the time-average and fluctuation,

$$f(\vec{r}, t) = \bar{f}(\vec{r}) + \tilde{f}(\vec{r}, t), \quad (5)$$

For cylindrically-symmetric configuration it is also useful to separate f into azimuthally symmetric and asymmetric components,

$$f(\vec{r}, t) = \langle f(\vec{r}, t) \rangle + \{f(\vec{r}, t)\}, \quad (6)$$

where $\langle f \rangle = (1/2\pi) \int f d\theta$ and $\{f\} = f - \langle f \rangle$ is the residual.

Based on the ergodic hypothesis, it is assumed that the time-average \bar{f} is equal to the azimuthal-average $\langle f \rangle$, and statistical moments of \tilde{f} and $\{f\}$ are equal. This separation of the variables into an axisymmetric and non-axisymmetric part does not preclude full non-linear solution, but it allows easier control over the background profiles of density, temperature and other quantities.

In turbulence where the eddy size is much smaller than the macroscopic system size, the separation of spatial scales leads to separation of time-scales for the evolution of local and spatially average fields. The turbulence diffusion coefficient can be estimated as,

$$D \sim l^2/\tau, \quad (7)$$

where l and τ are the spatial and temporal correlation scales for turbulent eddies; and the macroscopic evolution time is

$$T \sim L^2/D \sim (L/l)^2\tau \gg \tau \quad (8)$$

In spite of the separation of the time-scales the average and fluctuating quantities are certainly coupled since the average profile gradients provide the source of free energy driving turbulence; on the other hand, turbulent transport, along with sources, leads to evolution of the macroscopic profiles. If no sources are present in the simulation, the profiles relax to smaller gradient (Fig. 1).

3.2 Profile maintenance: suppressing the azimuthal average

Following self-consistent time evolution of turbulence and macroscopic transport may be difficult because the time-scale separation can make such calculations too large to be practical. Another problem is including correct source terms, which may involve atomic physics, radiation transport etc, and may be beyond the realm of the model.

Without attempting a self-consistent time evolution of turbulence and macroscopic transport one can consider intermediate time-scales $\tau \ll t \ll T$, where the macroscopic profiles can be taken as “frozen”, based on known measured experimental average profiles. In this case the time-evolution of only the non-axisymmetric part is considered, and a simple technique of maintaining the desired average profile is filtering out the axisymmetric part of evolving fields. This is illustrated in Fig. (2-3) showing the general appearance of ϕ , δn_i , and the evolution of the density and potential fluctuation RMS in a simulation with “frozen” density profile. In Fig. (3), the potential is split into the turbulence-generated axisymmetric component $\langle \phi \rangle$, and the non-axisymmetric residual $\{\phi\} = \phi - \langle \phi \rangle$. One can observe development of a zonal flow component $\langle \phi(r) \rangle$ corresponding to sheared azimuthal flow, which saturates the turbulence.

The easiest way to control the average profile is to suppress the evolution of the axisymmetric component by subtracting the azimuthal average of the right-hand side of the Eqs. (1-3):

$$\partial_t N = RHS - \langle RHS \rangle_\theta \quad (9)$$

This is effectively introducing a time-dependent source/sink function necessary to maintain exactly the target density profile.

Suppressing the axisymmetric part of fluctuations may interfere too much with the solution, and one can consider doing this not in the full domain but only on the boundary. This would constrain the boundary values, and may be enough to maintain the average profile close to the desired.

3.3 Profile maintenance: adding sources

A more "physical" method is using a source/sink term $S(r)$ designed in such a way that the average profile is maintained close to the desired function.

As a first step we use the method of subtracting out the azimuthal average to maintain the $\langle N_i \rangle$ profile close to the "target" density profile $N_{i0}(r)$, which is based on a representative experimental probe measurements in LAPD. Obtaining a steady-state turbulence solution we calculate the radial particle flux from fluctuating density and potential,

$$\Gamma = \langle N_i V_{Er} \rangle \quad (10)$$

Next, we calculate the effective volumetric density source $S(r)$ as

$$S = \nabla \cdot \Gamma \quad (11)$$

that can now be added to the density evolution equation, Eq. (1):

$$\partial_t N = RHS + S(r) \quad (12)$$

If needed, another iteration can be made by adjusting the source term to account for the mismatch between the current profile and the target. A more comprehensive approach to self-consistent time-evolution of turbulence and average profiles can be based on adding an adaptive source [17]; however it is beyond the scope of this paper. In our study extra iterations were not necessary; a single step was enough to produce stationary turbulence with average density profile close to the target profile (Fig. 4).

3.4 Effective diffusion coefficient

One can calculate the effective diffusion coefficient by dividing the radial flux by the gradient of the equilibrium density,

$$D_{eff} = -\frac{\Gamma}{\nabla N_{i0}} \quad (13)$$

The profiles of average radial flux and effective diffusion coefficient are shown in Fig. (5). One can observe that the resulting D_{eff} appears to be on the order of D_{Bohm} .

4 Comparison with LAPD data

Before any attempt is made to construct a full simulation of LAPD that self-consistently incorporates transport, sources/sinks and profile evolution, we need to ensure that the basic characteristics of the turbulence are correctly captured by the physical model we are using. We validate the application of BOUT to LAPD simulations by comparing the simulated data to the quantities readily available from LAPD measurements. The main experimental dataset used in this work is the data obtained by using a combination of fixed and moving Langmuir probes. The measured ion saturation current $I_{i,sat}$ fluctuations provide the information about the temporal and spatial characteristics of the turbulence.

To be able to compare turbulence characteristics to the measured data for the experimentally relevant plasma parameters, the average profiles have to be maintained close to the experimental values during the simulation. To do so, we apply the two methods described in section 3.2, either subtracting the azimuthal average of the right-hand side of the density equation, or adding a time-independent source function $S(r)$ to the right-hand side of Eq. (1).

Using these two methods, we simulate a steady-state turbulence for LAPD parameters, solving Eqs. (1-4) with the average density close to the experimental profile, for a range of ion-neutral collisionalities ($\nu_{in}/\Omega_{ci} = 2 \times 10^{-4}, 1 \times 10^{-3}, 2 \times 10^{-3}$). The estimated value for LAPD, based on neutral density $n_n \sim 5 \times 10^{11} \text{ cm}^{-3}$, is $\nu_{in}/\Omega_{ci} = 2 \times 10^{-3}$. As a first step, the electron temperature is not evolved and is taken as $T_e = 5 \text{ eV}$ in these simulations. The simulations are performed in the radial interval $0.15 \leq r \leq 0.45 \text{ m}$, in an azimuthal segment of a cylinder of $\pi/4$ angle. The grid size is $50 \times 32 \times 32$ points for radial, azimuthal and parallel directions. In order to improve the statistics, a series of uncorrelated runs is made with slightly different initial perturbations. To remove the slow variation of the average density observed in the experimental data that is not allowed in the simulations with fixed background profile, we apply the same temporal smoothing of the signal to the LAPD and BOUT data, which cuts off all frequencies below 800 Hz.

4.1 Fluctuations: temporal and spatial characteristics, pdf, skewness

The analysis of BOUT results shows that the $I_{i,sat}$ fluctuation amplitudes in LAPD data and the simulations have similar radial location near the cathode edge, where the background density gradient is largest (Fig. 6). The absolute values of the fluctuations are of the same order of magnitude, with simulated amplitudes smaller by a factor $\lesssim 2$ than the experimental data.

We now compare the frequency power spectrum of the density fluctuations $\delta n/n$ integrated over the volume $0.19 \leq r \leq 0.25$ m, using a sliding Hanning window for averaging between the different simulation runs (Fig. 7). Note that the total power in each spectrum is normalized to obtain the best fit to the experimental data. The slope of the simulated spectra is in agreement with the LAPD measurements in a range of frequencies that spans almost 2 orders of magnitude, for a range of ν_{in} values. As a check of numerical convergence, the spectrum for $\nu_{in}/\Omega_{ci} = 2 \times 10^{-3}$ is calculated with four times the size of the azimuthal extent of the grid and the number of azimuthal grid points ($N_z = 128$). The result is very similar to the original calculation, with a smaller grid size (Fig. 7, b and c).

Another important characteristic of the turbulence is the distribution of the fluctuation amplitudes. We calculate the PDF of $\delta n/n$ fluctuations from the LAPD moving probe data integrated over a volume of plasma $0.19 \leq r \leq 0.25$ m and compare it with the PDF from BOUT simulation in the same volume (Fig. 8). There are no normalizations or fit factors involved in this comparison. The experimental and the simulated PDFs are similar, with the average relative fluctuation $\langle |\delta n/n| \rangle$ of 0.11 for the measured data and 0.09, 0.10, 0.07 for BOUT simulations with $\nu_{in}/\Omega_{ci} = 2 \times 10^{-4}, 1 \times 10^{-3}, 2 \times 10^{-3}$.

Intermittent turbulence is observed in the edge plasmas of many experimental devices. This intermittency is usually attributed to generation and transport of coherent filaments of plasma, “blobs” or “holes” []. One signature of the presence of these structures is the non-zero skewness of the density fluctuation PDF. Typically, positive skewness associated with the “blobs” convectively transported outwards is observed in LAPD measurements in the region outside the cathode. Smaller negative values, associated with the “holes” are usually observed inside the cathode radius. The radial profile of the skewness of δn is shown in Fig. 9. Except for the edge of the simulation domain which

is affected by the imposed boundary conditions, the trend of the skewness profile, as well as the absolute values, is similar in BOUT simulations and in the LAPD data.

The simultaneous measurements of $I_{i,sat}$ by the fixed and the moving probes in LAPD allow to analyze the spatial structure of the turbulence. The moving probe in LAPD scans a plane perpendicular to the axis of the device for a large number of identical discharges. The reference probe remains at a fixed position that is close enough to the moving probe in the axial direction so that the parallel variation of the turbulent structures can be neglected. This allows to obtain the 2D spatial correlation function in the azimuthal plane. We construct a similar “synthetic” diagnostic to post-process BOUT simulation results by calculating the correlations between a reference location and all other points in each azimuthal plane. The correlation length in BOUT simulation is of the same order, but larger than the measured value (Fig. 10).

4.2 Fluxes and sources vs. inferred source/sink in LAPD

We now present an analysis of the inferred particle source that is required to maintain the density profile close to the experimental values, as described in section 3.3. The source function $S(r)$ appears to be positive inside $r_0=25$ cm, and negative outside (Fig. (11)). Remarkably, the qualitative form and magnitude of the $S(r)$ profile is consistent with the assumption that within $\sim r_0$ there is an ionization source, and outside of $\sim r_0$ there is a sink due to parallel streaming to the end walls. In LAPD, the field lines inside $r \sim 28$ cm connect to the cathode that produces the primary ionizing electron beam. The magnitude of the inferred source is close to the estimated ionization source and parallel losses sink for LAPD plasma, $S_{source} \sim n_n n_e \langle \sigma v \rangle_i \sim 2 \times 10^{20} \text{ m}^{-3}/s$ and $S_{sink} \sim n_i C_s / L_{\parallel} \sim 5 \times 10^{20} \text{ m}^{-3}/s$.

5 Discussion

5.1 Previous modeling of linear devices

In the past few years there have been several computational studies of linear plasma devices using fluid, or gyro-fluid, models. In a study [8] the importance of ion-neutral collisions was pointed out, which is consistent with our

results. In numerical studies [10, 18, 11] the formation and propagation of turbulent structures were investigated; it was reported that the simulation was able to reproduce the main experimental features. However, the present study is distinct by showing a detailed comparison with a range of experimental data.

5.2 Plasma transport

We have seen in section 4.1 that the simulated plasma turbulence has features that are usually associated with intermittency: non-Gaussian fluctuations, as seen by standard statistical moments - skewness and kurtosis. However, as we've seen in section 3.4 the turbulence-driven radial particle flux appears to be close to diffusive, $\Gamma = -D\nabla \langle n \rangle$, with the diffusion coefficient close to the Bohm value. This illustrates that “intermittent transport” and “non-diffusive transport” are not synonymous.

5.3 Similarity to tokamak edge turbulence

Usually edge turbulence has a broadband character, with characteristics similar in the edge of toroidal fusion devices (tokamaks, stellarators, and RFPs), magnetized toroidal plasmas without plasma current and flux surfaces, and linear devices, see review paper [19] and references therein. However, in some cases, edge instability is dominated by one, or a few, discrete modes, in linear devices [20, 21], and in tokamaks [22, 23].

For broadband edge turbulence, the power spectrum of broadband edge turbulence has a “universal” form, with a plateau region for low- f and a power-law decay $1/f^{2-4}$ [19]. This feature, also seen in the LAPD data, is reproduced in our simulations, see Fig.(7).

Statistical properties of edge turbulence, such as the skewness, are often used as indication of the turbulence intermittency [19]. In tokamak edge, the skewness is positive in the SOL (i.e. dominated by large amplitude events), but is sometimes negative inside the separatrix or limiter radius (i.e. with density “holes”), e.g. seen in DIII-D [24] and NSTX [25]. This feature is similar to LAPD data, and reproduced in our simulations, see Fig.(9).

Transport by large intermittent events, or “blobs”, may explain the properties of edge turbulence in toroidal devices, see [19, 26] and references therein. For linear plasmas the picture of curvature-driven blobs does not apply. A model of “neutral wind” has been proposed as a possible mechanism of blobs

motion [27] in linear plasmas. In our model there is no neutral wind, on the other hand, there is a centrifugal force due to the zonal flow which may also be a mechanism supporting the radial blob motion [26]. The role of coherent structures transport and mechanism of their motion in our simulations is the subject of ongoing investigation.

6 Conclusions

A numerical 3-D model of plasma turbulence is applied to LAPD. The physics model includes equations for plasma density, electron parallel momentum, and current continuity, for partially ionized plasma. The model is implemented in the numerical code BOUT.

In numerical calculations is observed self-consistent evolution of turbulence and self-generated electric field and zonal flows. Calculations closely reproduce experimental temporal spectra and are also consistent with the measured spatial structure and distribution of fluctuations amplitude.

Turbulent particle flux appears to be close to diffusive, with diffusion coefficient close to D_{Bohm} , and is consistent with estimates of density sources and sinks based on experimental data.

Appendices

A Ion viscosity

Including the ion-ion viscosity effects results in an additional term in the vorticity equation (3). Viscous force $\nabla \cdot \Pi$ (where Π is the stress tensor $\mathbf{v}\mathbf{v} - v^2/3\hat{\mathbf{I}}$) in the ion motion equation induces a perpendicular drift $\mathbf{v}_{i\perp\mu} = \mathbf{b} \times (\nabla \cdot \Pi)$ to the lowest order, which translates into an additional perpendicular current component $\mathbf{j}_{\perp,\mu} = en\mathbf{b} \times (\nabla \cdot \Pi)$. To simplify the final form of the viscous term, we will assume that density perturbations are small and the equilibrium gradients are negligible compared to the perturbed quantities. Then the extra term due to viscosity in the vorticity equation can be written as

$$\nabla \cdot j_{\perp,\mu} = en\nabla \cdot \{\mathbf{b} \times (\nabla \cdot \Pi)\} = -en\mathbf{b} \cdot \{\nabla \times (\nabla \cdot \Pi)\} \quad (14)$$

Using Braginskii expressions for the stress tensor [28] with perpendicular ion velocity $\mathbf{v}_{i\perp} = \mathbf{v}_E = \mathbf{b} \times \nabla\phi$ to the lowest order, it can be shown that the extra term in the vorticity equation (3) is $\mu_i \nabla_{\perp}^2 \varpi$.

Depending on the ion magnetization, one should choose either the magnetized or unmagnetized viscosity expression for the coefficient μ_i : $\mu_i = \eta_1^i = 0.3nT_i/\Omega_{ci}^2\tau_i$ for $\Omega_{ci}\tau_i \gg 1$ or $\mu_i = \eta_0^i = 0.96nT_i\tau_i$ for $\Omega_{ci}\tau_i \ll 1$. The estimate of the ion magnetization parameter $\Omega_{ci}\tau_i$ for typical LAPD values (He⁴, $B_0 = 400$ G, $n_i \sim 3 \times 10^{18}$ m⁻³, $T_i \sim 1$ eV) is close to unity. The ion temperature in LAPD is not directly measured; the estimate from the electron-ion energy exchange and the parallel losses balance indicates that T_i is in the range 0.1 – 1 eV. BOUT simulations with ion viscosity are consistent with the experimental measurements for low ion temperatures, $T_i \sim 0.1$ eV, which corresponds to unmagnetized ion regime.

B Discretization in the parallel coordinate

Consider the drift mode dispersion relation for the simplest case, without electron inertia and electromagnetic terms, when it becomes a quadratic equation

$$(\hat{\omega} - 1)i\hat{\sigma}_{\parallel} + \hat{\omega}^2 = 0, \quad (15)$$

where

$$\sigma_{\parallel} = \left(\frac{k_{\parallel}}{k_{\perp}}\right)^2 \frac{\Omega_{ci}\omega_{ce}}{0.51\nu_{ei}}, \quad (16)$$

and “hat” denotes normalization to ω_* ,

$$\omega_* = k_{\perp}v_{pe} = k_{\perp} \frac{V_{te}^2}{\omega_{ce}L_N} \quad (17)$$

as given in elementary plasma textbooks, e.g., [29].

Now consider the effect of finite-difference discretization on Eq. (15). For simplicity assume no radial structure so that the radial part of the solution can be dropped. There are just two coordinates then - the poloidal angle y and toroidal angle z .

Now let’s focus on the parallel discretization. Parallel derivatives that are represented by ik_{\parallel} in the Fourier form will become something different in the

discretized equation, depending on the type of discretization. For example, applying the 2nd central difference for a single mode $\exp(Ik_{\parallel}s)$ one obtains

$$\frac{df}{ds} \rightarrow \frac{\exp(Ik_{\parallel}s_{i+1}) - \exp(Ik_{\parallel}s_{i-1})}{2h} = \frac{I \sin(k_{\parallel}h)}{h} \quad (18)$$

Here s is the parallel coordinate, h is parallel grid spacing, $s_i = ih$.

One can notice that at large wavenumbers, $k \sim \pi/h$, the finite-difference representation is very poor. In our example, from Eq. 15, for $\hat{\sigma}_{\parallel} \gg 1$ the growth rate scales as $\gamma \propto 1/k_{\parallel}^2$, i.e., large k_{\parallel} should stabilize the modes. Conversely, in the discretized dispersion relation it will become $\gamma \propto 1/(\sin(kh))^2$ which would become singular at the Nyquist wavenumber $k = \pi/h$, which can be manifested in unphysical behavior of such modes. The possibility of unphysical behavior of high- k modes caused by spatial discretization, in particular the “red-black” numerical instability, is well-known in the CFD community, and historically the main remedy was using staggered grid [30]. A more recent popular method is discretization on collocated grids adding a dissipative biharmonic (i.e. 4th derivative) term to suppress the “red-black” instability (e.g., the Rhie-Chow interpolation).

Consider the effects of staggered grid for the discretized drift mode dispersion relation. Assume that N_i , ϕ , ϖ are specified on one grid, and j_{\parallel} , $V_{\parallel e}$ are specified on another grid shifted by $h/2$.

The k_{\parallel}^2 in the dispersion relation (15) can be tracked down to the derivatives

$$\frac{\partial j_{\parallel}}{\partial \parallel} \rightarrow (j_{\parallel,i} - j_{\parallel,i-1})/h = \exp(-Ikh/2) \frac{I \sin(kh/2)}{h/2} \quad (19)$$

and

$$\frac{\partial \phi_{\parallel}}{\partial \parallel} \rightarrow (\phi_{i+1} - \phi_i)/h = \exp(Ikh/2) \frac{I \sin(kh/2)}{h/2}, \quad (20)$$

which combine to produce

$$k_{\parallel}^2 \rightarrow - \left(\frac{\sin(kh/2)}{h/2} \right)^2 \quad (21)$$

One can note that Eq. (21) does not become zero for any mode supported by the grid, $-\pi/h \leq k \leq \pi/h$, which is an important improvement.

Since the staggered grid approach is more cumbersome for implementation, in particular for parallel computation, it is desirable to stay with collocated

grids, if possible. In our example one can come up with discretization Eq. (19,20) on collocated grids by combining right-sided and left-sided 1st order discretization. We call this method “quasi-staggered” grid.

Acknowledgements

Work performed for U.S.D.O.E. on the UCLA Basic Plasma Science Facility, which is supported by US DOE and US NSF; and by LLNL under Contract DE-AC52-07NA27344.

References

- [1] A. Hasegawa and K. Mima. *Physics of Fluids*, 21:87–92, 1977.
- [2] A. Hasegawa and K. Mima. *Phys. Rev. Lett.*, 39:205, 1978.
- [3] A. Hasegawa and M. Wakatani. *Phys. Rev. Lett.*, 59:1581, 1987.
- [4] W. Gekelman, H. Pfister, Z. Lucky, J. Bamber, D. Leneman, and J. Maggs. Design, construction and properties of the large plasma research device - the lapd at ucla. *Rev. Sci. Inst.*, 62:2875, 1991.
- [5] C M Franck et al. *Physics of Plasmas*, 10:323–325, 2003.
- [6] M J Burin et al. *Physics of Plasmas*, 12:052320, 2005.
- [7] S Shinohara et al. *Plasma Phys. Control. Fusion*, 37:1015, 1995.
- [8] Naohiro Kasuya, Masatoshi Yagi, Masafumi Azumi, Kimitaka Itoh, and Sanae-I. Itoh. *Journal of the Physical Society of Japan*, 76:044501, 2007.
- [9] C Holland, G R Tynan, J H Yu, A James, D Nishijima, M Shimada, and N Taheri. Numerical simulation of collisional drift-wave turbulence in a magnetized plasma column. *Plasma Phys. Control. Fusion*, 49:A109, 2007.
- [10] V Naulin, T Windisch, and O Grulke. Three-dimensional global fluid simulations of cylindrical magnetized plasmas. *Physics of Plasmas*, 4:012307, 2008.
- [11] T Windisch, O Grulke, R Schneider, and G N Kervalishvili. Formation and propagation of turbulent structures in drift-wave turbulence. *Contrib. Plasma Phys.*, 48(1-3):58–62, 2008.
- [12] J. E. Maggs, T. A. Carter, and R. J. Taylor. Transition from Bohm to classical diffusion due to edge rotation of a cylindrical plasma. *Physics of Plasmas*, 14(5):052507, May 2007.
- [13] T A Carter and J E Maggs. Modifications of turbulence and turbulent transport associated with a bias-induced confinement transition in the large plasma device. *Physics of Plasmas*, 16:012304, 2009.

- [14] P. Popovich, M.V. Umansky, T. A. Carter, and B. Friedman. Analysis of plasma instabilities and verification of bout code for linear plasma device LAPD, 2010. to be submitted for publication.
- [15] X Q Xu and R H Cohen. Scrape-Off Layer Turbulence Theory and Simulations. *Contrib. Plasma Phys.*, 36(1-2):158, 1998.
- [16] M.V. Umansky, X.Q. Xu, B. Dudson, L.L. LoDestro, and J.R. Myra. Status and verification of edge plasma turbulence code BOUT. *Contrib. Plasma Phys.*, 180:887–903, 2009.
- [17] B. Dudson. private communication, 2009.
- [18] Kervalishvili G N et al. Intermittent turbulence in the linear vineta device. *Contrib. Plasma Phys.*, 48:32, 2008.
- [19] Zweben S J et al. Recent theoretical progress in understanding coherent structures in edge and sol turbulence. *Plasma Phys. Control. Fusion*, 49:S1, 2007.
- [20] T Windisch et al. *Physics of Plasmas*, 13:122303, 2006.
- [21] Chiu J S et al. *Physics of Plasmas*, 7:4492, 2000.
- [22] Snipes J A et al. *Plasma Phys. Control. Fusion*, 43:L23, 2001.
- [23] Burrell K H et al. *Plasma Phys. Control. Fusion*, 44:A253, 2002.
- [24] Boedo J A et al. Transport by intermittency in the boundary of the diiii-d tokamak. *Physics of Plasmas*, 10:?, 2003.
- [25] Boedo J A et al. *Physics of Plasmas*, 8:4826, 2001.
- [26] Krasheninnikov S I et al. Recent theoretical progress in understanding coherent structures in edge and sol turbulence. *J. Plasma Physics*, 74:679, 2008.
- [27] Krasheninnikov S I and Smolyakov A I. *Physics of Plasmas*, 10:3020, 2003.
- [28] S I Braginskii. Transport processes in a plasma. In M A Leontovich, editor, *Reviews of Plasma Physics*, volume 1, pages 205–311. Consultants Bureau, New York, 1965.

- [29] Francis F. Chen. *Introduction to Plasma Physics and Controlled Fusion*. Plenum Press, New York, 1984.
- [30] Suhas V. Patankar. *Numerical Heat Transfer and Fluid Flow*. Hemisphere Publishing Corporation, New York, 1980.

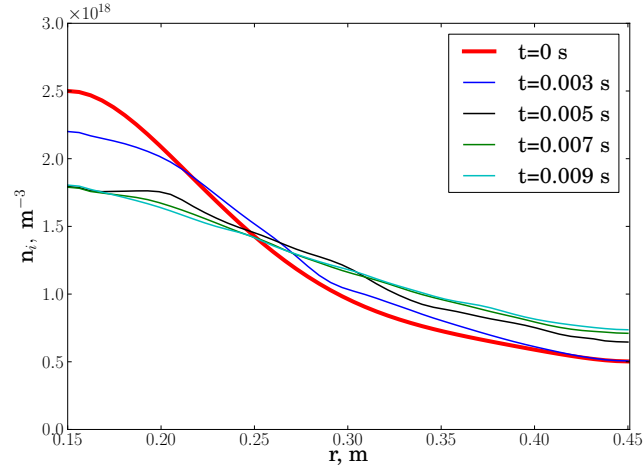


Figure 1: *Relaxation of the density profile in a simulation without sources.*

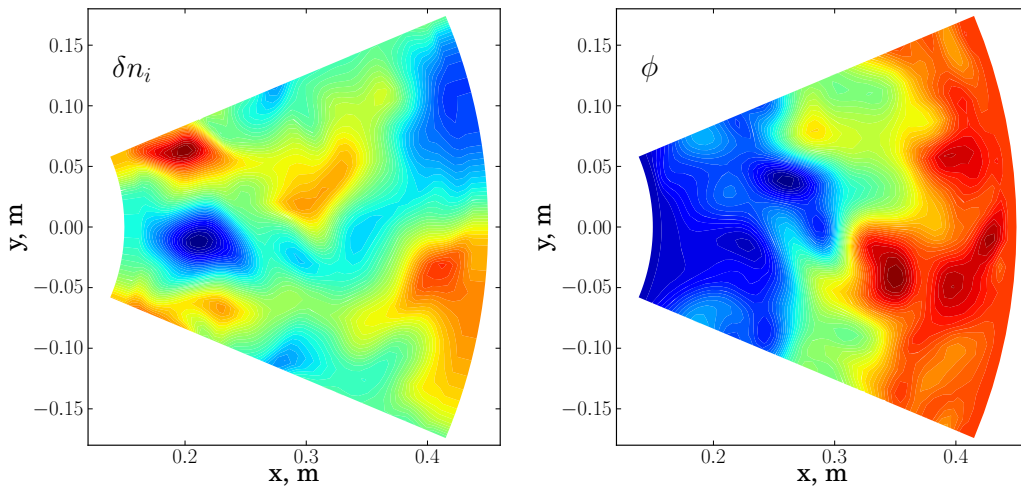


Figure 2: *Spatial structure of the perturbed density (left) and turbulence-generated potential (right) at $t = 5.2$ ms.*

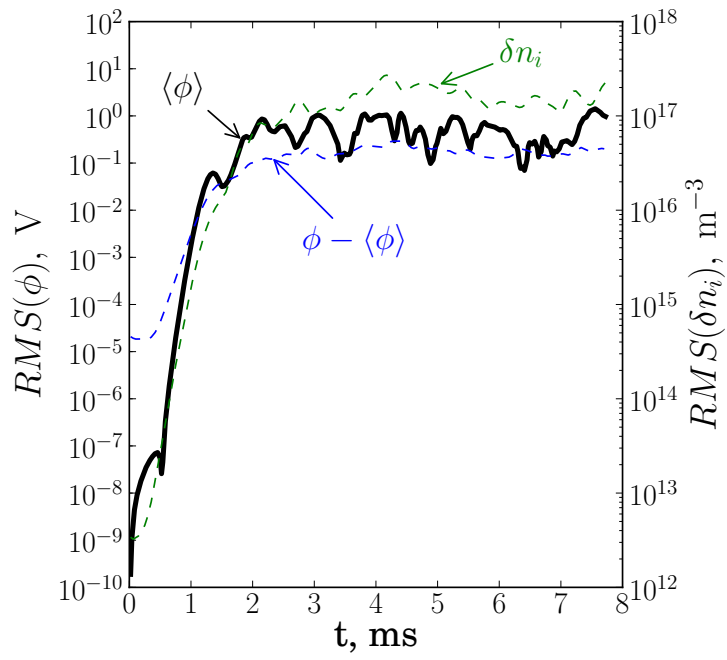


Figure 3: *Time evolution of the density and potential fluctuation RMS in a typical simulation. The potential is split into the axisymmetric ($\langle\phi\rangle$, zonal flow component) and the non-axisymmetric ($\phi - \langle\phi\rangle$) components.*

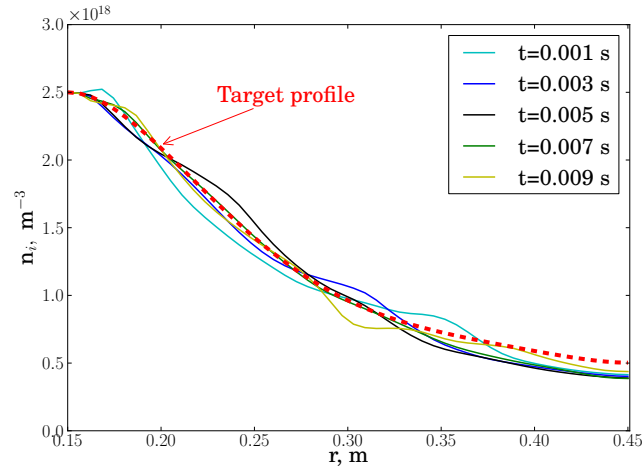


Figure 4: Instantaneous density profile $\langle N_i \rangle$ in simulation with density source $S(r)$.

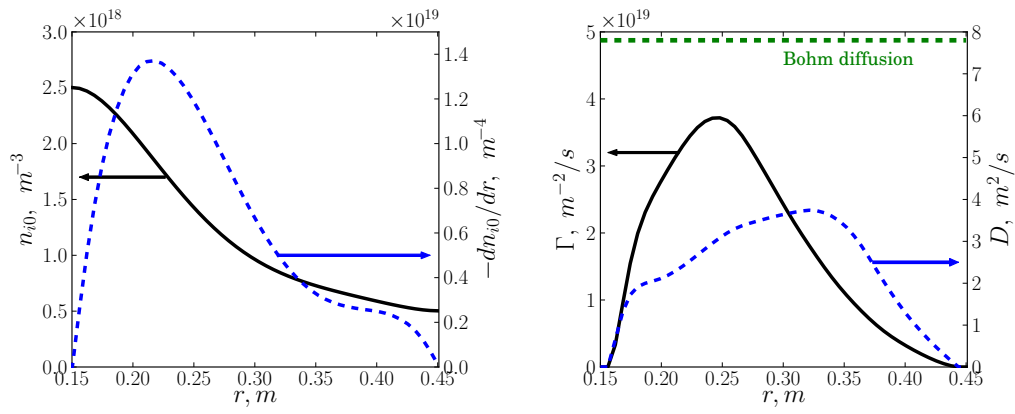


Figure 5: Left: Radial profiles of average n_i and dn_i/dr . Right: radial particle flux Γ and the effective diffusion coefficient D .

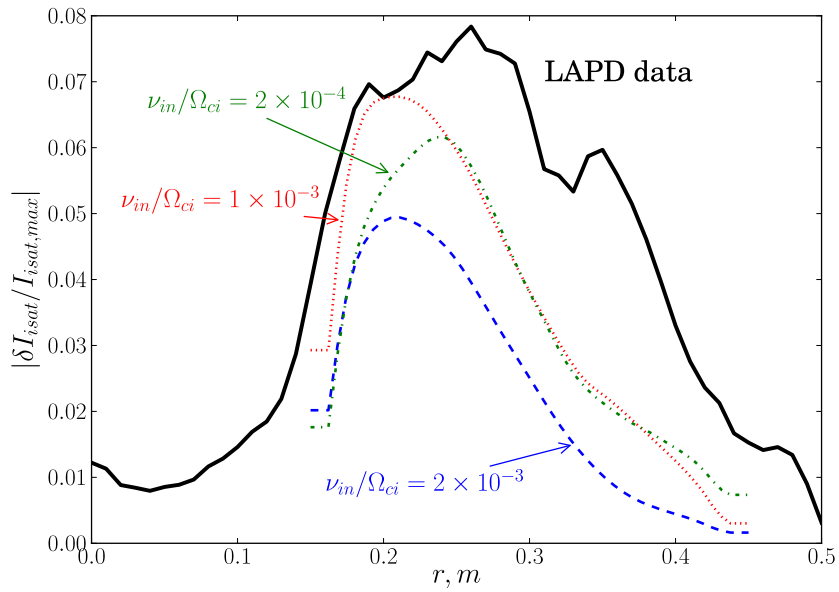


Figure 6: Radial distribution of the average ion saturation current fluctuations normalized to the maximum equilibrium profile value.

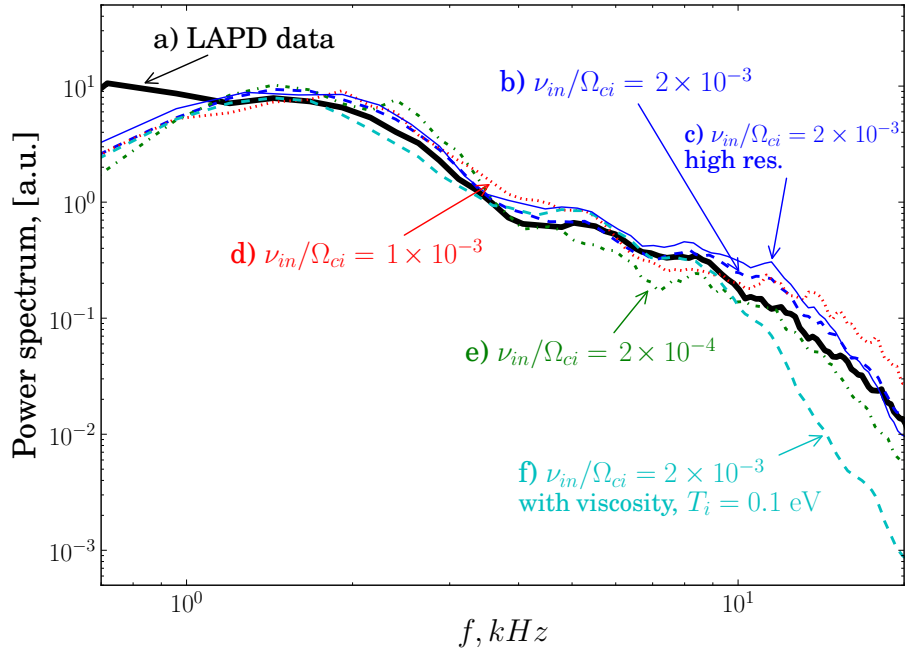


Figure 7: Frequency power spectrum of the density fluctuations: LAPD measurements (a) and BOUT simulations (b-f) for b) $\nu_{in}/\Omega_{ci} = 2 \times 10^{-3}$, c) $\nu_{in}/\Omega_{ci} = 2 \times 10^{-3}$ with $N_z = 128$ azimuthal grid size, d) $\nu_{in}/\Omega_{ci} = 1 \times 10^{-3}$, e) $\nu_{in}/\Omega_{ci} = 2 \times 10^{-4}$, f) $\nu_{in}/\Omega_{ci} = 2 \times 10^{-3}$ with ion viscosity at $T_i = 0.1$ eV. Experimental density profile, $T_e = 5$ eV.

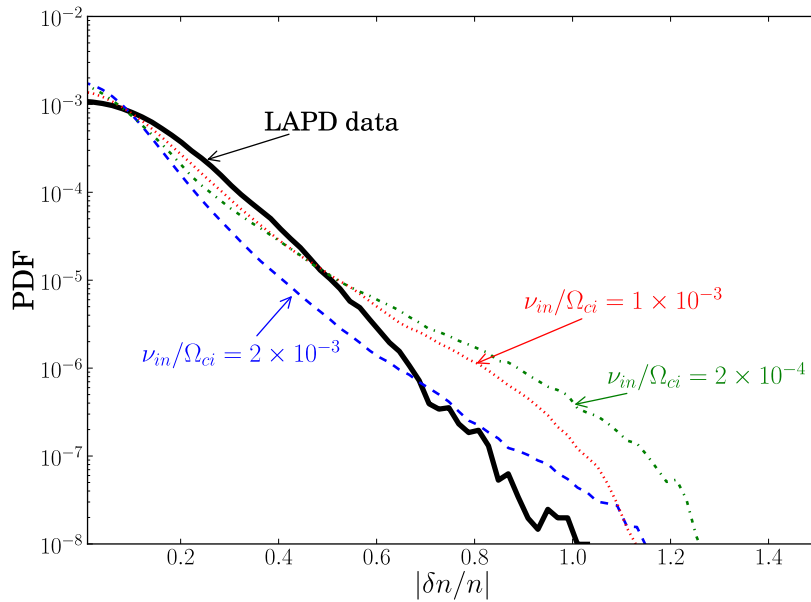


Figure 8: *Probability distribution function of $\delta n/n$ fluctuation amplitude in BOUT simulations and LAPD data. PDF is volume averaged in the interval $0.19 \leq r \leq 0.25$ m.*

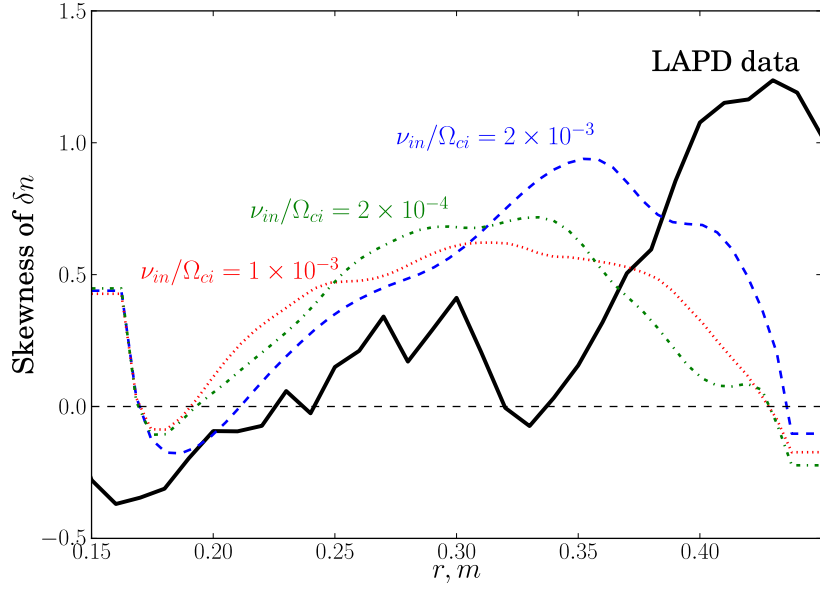


Figure 9: *Skewness of δn distribution in BOUT simulations and LAPD measurements.*

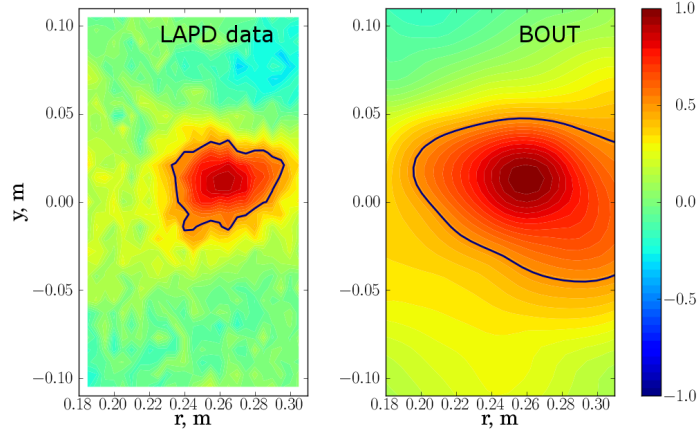


Figure 10: Correlation function for $I_{i,sat}$ fluctuations measured using a moving probe.

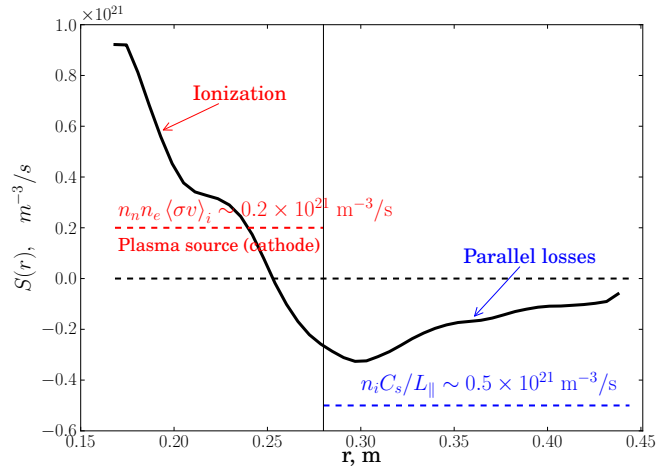


Figure 11: Inferred particle source required to maintain the measured density profile.